

Robust universal relations in neutron star asteroseismology

Deepak Kumar ^{1,2}, Tuhin Malik ³, Hiranmaya Mishra ^{1,4} and Constança Providência ³

¹Theory Division, Physical Research Laboratory, Navarangpura, Ahmedabad 380 009, India

²Indian Institute of Technology Gandhinagar, Gandhinagar 382 355, Gujarat, India *

³CFisUC, Department of Physics, University of Coimbra, PT 3004-516 Coimbra, Portugal[†]

⁴School of Physical Sciences, National Institute of Science Education and Research, Jatni, 752050 India[‡]

(Dated: June 16, 2023)

The non-radial oscillations of the neutron stars (NSs) have been suggested as an useful tool to probe the composition of neutron star matter (NSM). With this scope in mind, we consider a large number of equations of states (EOSs) that are consistent with nuclear matter properties and pure neutron matter EOS based on a chiral effective field theory (chEFT) calculation for the low densities and perturbative QCD EOS at very high densities. This ensemble of EOSs is also consistent with astronomical observations, gravitational waves in GW170817, mass and radius measurements from Neutron star Interior Composition Explorer (NICER). We analyze the robustness of known universal relations (URs) among the quadrupolar f mode frequencies, masses and radii with such a large number of EOSs and we find a new UR that results from a strong correlation between the f mode frequencies and the radii of NSs. Such a correlation is very useful in accurately determining the radius from a measurement of f mode frequencies in the near future. We also show that the quadrupolar f mode frequencies of NS of masses $2.0 M_{\odot}$ and above lie in the range ~ 2 -3 kHz in this ensemble of physically realistic EOSs. A NS of mass $2M_{\odot}$ with a low f mode frequency may indicate the existence of non-nucleonic degrees of freedom.

Introduction. The neutron star (NS) observations in the multi-messenger astronomy have piqued a lot of interest in the field of nuclear astrophysics and strong interaction physics. The recent radio, x-rays and gravitational waves (GWs) observations in the context of NSs have provided interesting insights into the properties of matter at high density. The core of such compact objects is believed to contain matter at few times nuclear saturation density, ρ_0 ($\rho_0 \approx 0.16 \text{ fm}^{-3}$) [1–4] and provides an unique window to get an insight into the behavior of matter at these extreme densities. On the theoretical side, no controlled reliable calculations are there that can be applicable to matter densities relevant for the NS cores. The lattice quantum chromodynamics (IQCD) simulations are challenging at these densities due to sign problem in Monte-Carlo simulations. On the other hand, the analytical calculations like chiral effective field theory (chEFT) is valid only at low densities while perturbative quantum chromodynamics (pQCD) is reliable at extremely high densities. In recent approaches, the equation of state (EOS)s between these two limits have been explored by connecting these limiting cases using a piecewise polytropic interpolation, speed of sound interpolation or spectral interpolation [5–11].

The NS properties such as mass, radius and quadrupole deformation of merging NSs can constrain the uncertainty in EOS. The discovery of massive NS with masses of the order of $2M_{\odot}$ requires the EOS to be stiff. However, the fact that non-nucleonic degrees of freedom soften the EOS at high density, puts a constraint on the EOS at the intermediate densities. The observations of GWs from binary neutron star (BNS) inspiral by Advanced LIGO and Advanced Virgo GWs observatories have opened a new window in the field of multi-messenger astronomy and nuclear physics. The inspiral phase of NS-NS merger leads to tidal deformation (Λ), which is strongly sensitive to the compactness. Since Λ is related to the EOS of the

neutron star matter (NSM), this measurement acts as another constraint on the EOS. On the other hand, recovering the nuclear matter properties from the EOS of β -equilibrated matter is rather non trivial. This further requires the knowledge of the composition (*e.g.* proton fraction) of matter at high densities [12–15].

In the context of GWs, the non-radial oscillations of NS are particularly interesting as they can carry information of the internal composition of the stellar matter. These oscillations in the presence of perturbations (electromagnetic or gravitational) can emit GWs at the characteristic frequencies of its quasi-normal mode (QNM). The frequencies of QNM depend on the internal structure of NS and it may be another probe to get an insight regarding the composition of NSM also known as asteroseismology. Different QNMs are distinguished by the restoring forces that act on the fluid element when it gets displaced from its equilibrium position. The important fluid modes related to GWs emission include fundamental (f) modes, pressure (p) modes and gravity (g) modes driven by the pressure and buoyancy respectively. The frequency of p modes is higher than that of g modes while the frequency of f modes lies in between. The focus of the present investigation is on the quadrupolar f modes that are correlated with the tidal deformability during the inspiral phase of NS merger [16] and have the strongest tidal coupling among all the oscillation modes. More importantly, these modes lie within the sensitivity range of the current as well as upcoming generation of the GWs detector networks [17]. In this context, QNMs have been studied with various EOS models and some universal/quasi-universal behaviors for the frequency and damping time which are insensitive to the EOS models [18–25]. This needs to be explored further regarding the robustness of these relations for a large number of EOSs consistent with recent observational constraints.

In this letter we propose two major points of interest. Firstly we estimate, within the Cowling approximation [26, 27], the f mode oscillation frequencies for NSs using a large number of EOSs and demonstrate that observation of f mode frequencies, apart from causality $c_s^2 \leq 1$ and maximum mass constraints, further restrict the EOSs. Secondly we verify the robustness of few universal relation (UR) among the quadrupolar f mode frequencies, masses and radii studied earlier with limited EOSs. It has been earlier found that these URs between NS properties are strongly violated by hybrid EOSs [28–30] and certain exotic phases [31]. We consider here a large number of EOSs and confirm that a known UR is almost insensitive to the EOSs, while a second one depends slightly on the composition of the EOSs, i.e. the presence or not of non-nucleonic degree of freedom, and, finally, we propose a new UR.

Setup - The two ensembles of EOSs that we consider here are constructed by stitching together EOSs valid for different segments in baryon densities. For the outer crust the Bethe-Pethick-Sutherland (BPS) EOS is chosen [32]. Outer crust and the core are joined using a polytropic form $p(\varepsilon) = a_1 + a_2\varepsilon^\gamma$ in order to construct the inner crust, where the parameters a_1 and a_2 are determined in such a way that the EOS for the inner crust matches with the outer crust at one end ($\rho = 10^{-4} \text{ fm}^{-3}$) and with the core at the other end ($\rho = 0.04 \text{ fm}^{-3}$). The polytropic index γ is taken to be $4/3$ [33]. It is important to note that the differences in NSs radii between this treatment of the inner crust EOS and the unified inner crust description including the pasta phases have been found to be less than 0.5 km, as discussed in [34]. The core EOSs are considered within two different approaches: (i) a nucleonic β -equilibrated EOS based on a relativistic description of hadrons through their density-dependent couplings constrained by the existing observational, theoretical and experimental data through a Bayesian analysis (DDB), obtained in [34], which satisfies pure neutron matter (PNM) constraints at low densities obtained from next-to-next-to-next-to leading order ($N^3\text{LO}$) calculations in the chEFT [35, 36]. (ii) a hybrid set of EOSs which consists of the DDB EOS at low density ($\leq 2\rho_0$) and the deconfined quark matter at very high densities ($\geq 40\rho_0$) while the region ($2\rho_0$ - $40\rho_0$) is interpolated by piecewise polytropes (DDB-Hyb). For the deconfined quark matter, we employ NNLO pQCD results of Refs. [6, 37] which can be cast in a simple fitting function for the pressure as a function of chemical potential (μ) given as

$$P_{\text{pQCD}}(\mu) = \frac{\mu^4}{108\pi^2} \left(c_1 - \frac{d_1 X^{-\nu_1}}{(\mu/\text{GeV}) - d_2 X^{-\nu_2}} \right) \quad (1)$$

where the parameters are $c_1 = 0.9008$, $d_1 = 0.5034$, $d_2 = 1.452$, $\nu_1 = 0.3553$ and $\nu_2 = 0.9101$ [38]. Here X is a dimensionless renormalization scale parameter, $X = 3\bar{\Lambda}/\mu$ which is allowed to vary $X \in [1, 4]$. We use this pQCD EOS for densities beyond $\rho \simeq 40\rho_0$ which corresponds to $\mu_{\text{pQCD}} = 2.6 \text{ GeV}$ [38]. Between the region of the validity of pQCD and DDB i.e. $\mu_{\text{DDB}} \leq \mu \leq \mu_{\text{pQCD}}$, where μ_{DDB} is the chemical potential of DDB EOS at $\rho = 2\rho_0$, we divide

the interval into two segments, $(\mu_{\text{DDB}} - \mu_c)$ and $(\mu_c - \mu_{\text{pQCD}})$, and assume EOS has a polytropic form in each segment i.e. $P_i(\rho_i) = \kappa_i \rho_i^{\gamma_i}$ for the i -th segment [37]. The segments can be connected to each other by requiring that the pressure and the energy density are continuous at μ_c as well as the pressure should be an increasing function of the energy density and the EOS must be subluminal. We also ensure that there is no jump in the baryon number density. This corresponds to assuming no first order phase transition between hadronic matter and quark matter. If one wishes to include a first order phase transition, an extra term to the number density at μ_c can be added [37].

To obtain the EOS of the core, we proceed as follows. For the outer core, which extends approximately until $\rho = 2\rho_0$, we use a soft (stiff) DDB EOS as obtained in Ref. [34] within 90% CI. The corresponding value of chemical potential at $\rho = 2\rho_0$ is $\mu_{\text{DDB}} = 1.036$ (1.097) GeV for a soft (stiff) DDB EOS. We interpolate the region from $\mu = \mu_{\text{DDB}}$ to $\mu = \mu_c$ and from $\mu = \mu_c$ to $\mu = \mu_{\text{pQCD}}$ with two piecewise polytropes. We select all those EOSs which (i) match with pQCD at $\mu = \mu_{\text{pQCD}}$ (i.e. $X \in [1, 4]$) (ii) have pressure as an increasing function of energy density, and (iii) are subluminal. We refer this EOS as DDB-Hyb. The chemical potential μ_c is here chosen in such a way that the EOS matches pQCD at $\mu = \mu_{\text{pQCD}}$. We take $\mu_c \in [1.04, 2.2]$ GeV and the corresponding pressure $P_c \in [20, 1260]$ MeV.fm $^{-3}$. For an ensemble of DDB-Hyb EOSs we choose μ_c, P_c randomly in the prescribed domain by Latin-Hypercube-Sampling method [39] for a uniform distribution. For a given μ_c, P_c and P_{DDB} , the parameters of the first polytrope, (κ_1, γ_1) get determined. Similarly for a given μ_c, P_c and P_2 (where P_2 is the pQCD pressure for a given value of X at $\mu = \mu_{\text{pQCD}}$), the parameters of the second polytrope (κ_2, γ_2) get determined. The domains for pressure (P_c) and chemical potential (μ_c) become $P_c \in [45, 1255]$ MeV.fm $^{-3}$ and $\mu_c \in [1.07, 2.09]$ GeV after constrained by pQCD. These domains further squeeze to $P_c \in [53, 680]$ MeV.fm $^{-3}$ and $\mu_c \in [1.15, 1.88]$ GeV after putting the constraint of $M_{\text{max}} \geq 2M_\odot$ and so we find 0.38 million EOSs out of 54 million sampled EOSs satisfying these constraints. It may be mentioned here that, although we use two polytropes for the interpolation between $(\mu_{\text{DDB}} - \mu_{\text{pQCD}})$, there have been different interpolation functions like spectral decomposition [40, 41] and speed of sound method [9, 11, 42].

Pulsating equations - To estimate the specific oscillation frequency of NSs, let us discuss the non-radial oscillation of a spherically symmetric NS characterized by the background space-time metric where the line element is given by

$$ds^2 = -e^{2\Phi} dt^2 + e^{2\Lambda} dr^2 + r^2 (d\theta^2 + \sin^2 \theta d\phi^2). \quad (2)$$

We shall consider the pulsating equations within the Cowling approximation so that our study is limited to the modes related to fluid perturbations and neglect the metric perturbations. The Lagrangian fluid displacement vector is given by

$$\xi^i = (e^{-\Lambda} W, -V \partial_\theta, -V \sin^{-2} \theta \partial_\phi) r^{-2} Y_{lm} \quad (3)$$

Where $W(r, t)$ and $V(r, t)$ are the perturbation functions and Y_{lm} are the spherical harmonic function. The perturbation equations that describe oscillations can be obtained by the perturbed Einstein field equations $\delta G_{\alpha\beta} = 8\pi\delta T_{\alpha\beta}$ with $G_{\alpha\beta} = R_{\alpha\beta} - \frac{1}{2}g_{\alpha\beta}R$ being the Einstein tensor. Linearising these equations in the perturbation, while choosing a harmonic time dependence for the perturbation i.e. $W(r, t) \propto W(r)e^{i\omega t}$ and $V(r, t) \propto V(r)e^{i\omega t}$ with frequency ω , the differential equations further fluid perturbation functions can be obtained as [24, 26, 43]

$$W' = \frac{d\epsilon}{dP} \left(\omega^2 r^2 e^{\Lambda-2\Phi} V + W\Phi' \right) - l(l+1)e^{\Lambda} V, \quad (4)$$

$$V' = 2V\Phi' - \frac{1}{r^2} W e^{\Lambda}, \quad (5)$$

here, the ‘prime’ denotes the total derivative with respect to r . These equations are solved with appropriate boundary conditions at the stellar center $r = 0$ and at the surface $r = R$. The W and V in the vicinity of the stellar center are taken as $W(r) \sim Cr^{l+1}$ and $V(r) \sim -Cr^l/l$, where C is an arbitrary constant. The other boundary condition that needs to be fulfilled is that the Lagrangian perturbation to the pressure must vanish at the stellar surface. This leads to [24, 26, 43]

$$\omega^2 r^2 e^{\Lambda-2\Phi} V + W\Phi' \Big|_{r=R} = 0 \quad (6)$$

This apart in the case of density discontinuity these equations have to be supplemented by an extra junction condition at the surface of discontinuity. We shall not consider here a density discontinuity. With these boundary conditions, the problem becomes an eigenvalue problem for the parameter ω which can be estimated numerically. We shall confine ourselves to $l = 2$ quadrupolar modes.

Results - We now proceed to analyze the ensembles of EOSs that are consistent with nuclear matter properties or PNM EOS based on theoretically robust chEFT at low densities and pQCD at very high densities. As mentioned earlier, we start with 54 million EOSs. We discard those EOS which do not match the two end points or are superluminal (square of speed of sound $c_s^2 > 1$) as well as the condition of positive speed of sound. This leaves us with an ensemble of 0.38 million DDB-Hyb EOSs. This ensemble of EOSs is represented in Fig. 1 by the orange band. We next enforce the $M_{\max} \geq 2.0M_{\odot}$ constraint resulting from solving the Tolman-Oppenheimer-Volkoff (TOV) equations with this ensemble. This constraint further reduces the number of EOSs to 55,000 which are displayed in Fig. 1 as the gray band, named here after DDB-Hyb set. The polytrope indices γ_1 and γ_2 are seen to vary over an intervals $\gamma_1 \in [1.67, 13.76]$ and $\gamma_2 \in [1.0, 1.51]$. The tight constraint on γ_2 has its origin on the matching to the pQCD pressure. In Fig. 1, the light blue band is the β -equilibrated nuclear matter $\approx 10k$ EOSs (DDB 90% CI) while the dark red band corresponds to pQCD EOS. For comparison, we also plot the domain of EOSs obtained in Ref. [10] (red solid curve) compatible with recent NICER and GWs observations. The red dashed lines refers to the dense

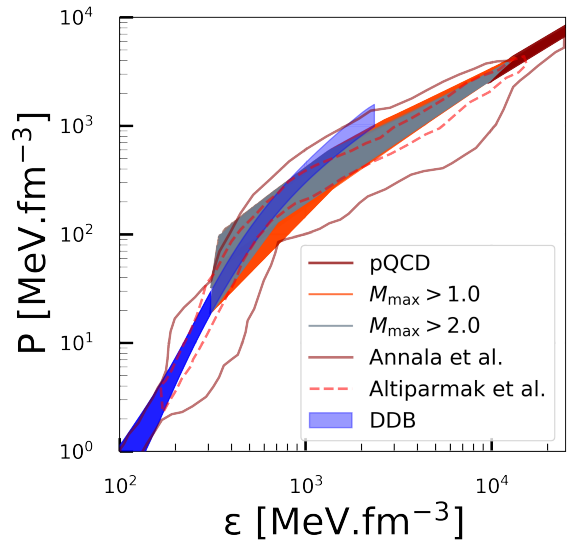


FIG. 1. We show pressure and energy density regions in MeV.fm^{-3} of our sampled EOSs (DDB and DDB-Hyb). We consider nucleonic β -equilibrated EOS of the 90% CIs for DDB (light blue) as a full range and (dark blue) up to $2\rho_0$ [34] and at very high density $\sim 40\rho_0$ the NNLO pQCD (dark red) [6]. In the intermediate region, EOS is evolved in thermodynamically consistent way with two polytropic segments (see text for details). Also included are the limits of the domain of EOSs obtained in Ref. [10] (red solid curve) and the dense PDF (≥ 0.08) calculated in Ref. [11] (red dashed lines).

PDF (≥ 0.08) obtained in Ref. [11] with continuous sound speed and consistent not only with nuclear theory and pQCD, but also with astronomical observations. It is to be noted that both of DDB and DDB-Hyb sets are compatible with them.

In Fig. 2, we plot the NS mass-radius and f mode frequency-mass regions obtained at 90% CI for the conditional probabilities $P(R|M)$ (left) and $P(f|M)$ (right) from the mass-radius clouds arising from the ensembles of EOSs of DDB-Hyb (black dotted) and DDB (dark red). The blue horizontal bar on the left panel indicates the 90% CI radius for a $2.08M_{\odot}$ star determined in Ref. [44] combining observational data from GW170817 and NICER as well as nuclear data. The top and bottom gray regions indicate, the 90% (solid) and 50% (dashed) CI of the LIGO/Virgo analysis for each binary component from the GW170817 event [45] respectively. The 1σ (68%) credible zone of the 2-D posterior distribution in mass-radius domain from millisecond pulsar PSR J0030+0451 (cyan and yellow) [46, 47] as well as PSR J0740 + 6620 (violet) [44, 48] are shown for the NICER x-rays data. The horizontal (radius) and vertical (mass) error bars reflect the 1σ credible interval derived for the same NICER data’s 1-D marginalized posterior distribution. The mass-radius domain for the DDB-Hyb set sweeps a wider range than the DDB set, restricted to nucleonic degrees of freedom. The DDB-Hyb set constrained by pQCD at high density leads to larger radii for high mass NS. We conclude that the present observational constraints either obtained from GW170817 or NICER cannot rule out the existence of exotic degrees of freedom. In

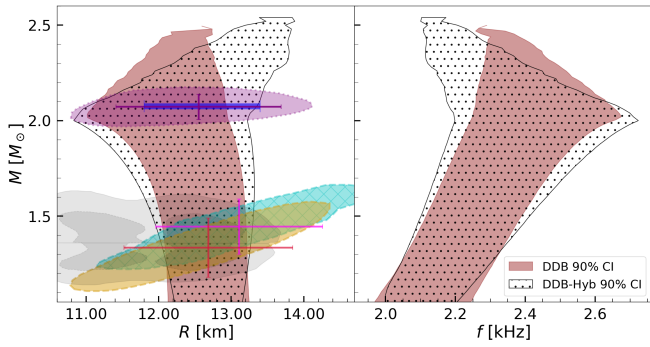


FIG. 2. NS mass (M)-radii (R) and f mode frequency-mass (M) region obtained from the 90% CI for the conditional probabilities $P(R|M)$ (left) and $P(f|M)$ (right) for DDB-Hyb (black dotted) and DDB (dark red). The blue horizontal bar on the left panel indicates the 90% CI radius for a $2.08M_{\odot}$ star determined in [44] combining observational data from GW170817 and NICER as well as nuclear saturation properties. The top and bottom gray regions indicate, respectively, the 90% (solid) and 50% (dashed) CI of the LIGO/Virgo analysis for each binary component from the GW170817 event [45]. The 1σ (68%) credible zone of the 2-D posterior distribution in mass-radii domain from millisecond pulsar PSR J0030+0451 (cyan and yellow) [46, 47] as well as PSR J0740 + 6620 (violet) [44, 48] are shown for the NICER x-rays data. The horizontal (radius) and vertical (mass) error bars reflect the 1σ credible interval derived for the same NICER data's 1-D marginalized posterior distribution.

the right panel, we see that the 90% CI for $P(f|M)$ f mode frequency $f \in [1.95, 2.7]$ kHz for both the DDB and DDB-Hyb sets. The range is smaller for low NS mass and as the mass increases the 90% CI for f mode frequency increases. The f mode frequency of a NS above $2M_{\odot}$ mass is in the range (2.1-2.7) kHz and (2.3-2.65) kHz for the DDB-Hyb and DDB sets, respectively. As mentioned in the earlier sections, the solutions for f mode obtained in this work are within the Cowling approximation (neglecting perturbations of the background metric). It was shown that the Cowling approximation can overestimate the quadrupolar f mode frequency of NSs by up to 30 to 10 % for NS masses in the range (1.0-2.5) M_{\odot} compared to the frequency obtained in the linearised general relativistic (GR) formalism [21, 49, 50]. The accurate measurement of f modes may further constrain EOS to a narrower range. Besides, a star of $2M_{\odot}$ with a low f mode frequency may indicate an existence of non-nucleonic degrees of freedom.

In Fig. 3, we have studied two known URs involving the f mode frequency with global properties of NS, often studied in literature with a limited set of EOSs. In particular, we name UR1 the UR between the f mode frequency and the square root of the average star density $\sqrt{M/R^3}$, and UR2a the UR involving the ωM versus the compactness M/R , where $\omega = 2\pi f$. We have analysed their robustness with our EOS sets, DDB-Hyb and DDB. We have also found a new and direct relation between the f modes frequency, f , and radius, R , with the help of the existing strong correlation between them.

In the left panel of the figure we show UR1:

$$f = a\sqrt{(M/R^3)} + b. \quad (7)$$

It has been shown in Refs. [19, 52] that the average density can be well parameterized via the f mode frequency. The following values of a and b have been obtained: $a = 22.27 \pm 0.023$ (26.76 ± 0.01) kHz.km, $b = 1.520 \pm 0.001$ (1.348 ± 0.001) kHz for DDB-Hyb (DDB). The maximum relative percentage error obtained for UR1 within 90% CI is 6.0%(4.5%) for DDB-Hyb (DDB). We verify that the UR1 depends slightly on the EOS, reflected in a relative dispersion of $\sim 5\%$ at 90%CI. Also, the slope of the medians depend on the dataset, with the nucleonic data set DDB presenting a 15% larger slope, and similar to the one obtained in [49] which was calculated with realistic nucleonic EOS, and is at the upper limit of our 90% CI. It is important to take note that this particular work has been executed utilizing the Cowling approximations [24, 26, 43] as previously referenced. In the scholarly publication by Yoshida et al. [51], a comparative analysis was performed between the outcomes obtained from complete linearized General Relativity (GR) and those acquired through the Cowling approximations. The findings of their study reveal that, for $l = 2$, the f mode is overestimated by 30% and 15% when the compactness values of M/R are 0.05 and 0.2, respectively. Using this as a linear relation, we have scaled the solutions obtained in the Cowling approximation, for both DDB and DDB-Hyb, see the bottom band in Fig. 3 left panel designated by GR solutions. It is interesting to notice that the scaled frequencies are compatible with the full GR solutions obtained in the literature. Notice that the dispersion is smaller, but still corresponds to a 5% relative uncertainty. In Andersson & Kokkotas (Benhar et al) the authors have obtained the following parameters $a = 35.9(33.0)$ kHz.km and $b = 0.78$ (0.79) kHz [19, 21, 52], the difference between both works being the EOS considered in the study. In those studies the linearised GR equations were solved, and, as expected, lower frequencies have been determined. In Ref. [49], the oscillations of non-rotating and fast rotating NSs have been explored with a different set of EOSs based on microscopic theories within the Cowling approximation. The values of the coefficients of the UR1 obtained were $a = 25.32$ kHz.km and $b = 1.562$ kHz, which are at the 90% CI upper limit of the relations we have obtained.

In center panel of the Fig. 3 we display UR2a:

$$\omega M = a \left(\frac{M}{R} \right) + b \quad (8)$$

obtained for both DDB-Hyb and DDB sets, with $a = 0.6474 \pm 4.6 \times 10^{-5}$ ($a = 0.6549 \pm 2.6 \times 10^{-5}$) and $b = -0.0085 \pm 1.05 \times 10^{-5}$ ($b = -0.0103 \pm 6.18 \times 10^{-6}$) for DDB-Hyb (DDB) set. Both the coefficients are dimensionless. The maximum relative percentage error obtained for UR2a within 90% CI is 3.78% (2.20%) for DDB-Hyb (DDB) set. The values of the slope and intercept for UR2a are also compatible with the ones obtained in Ref. [53] within the Cowling approximation

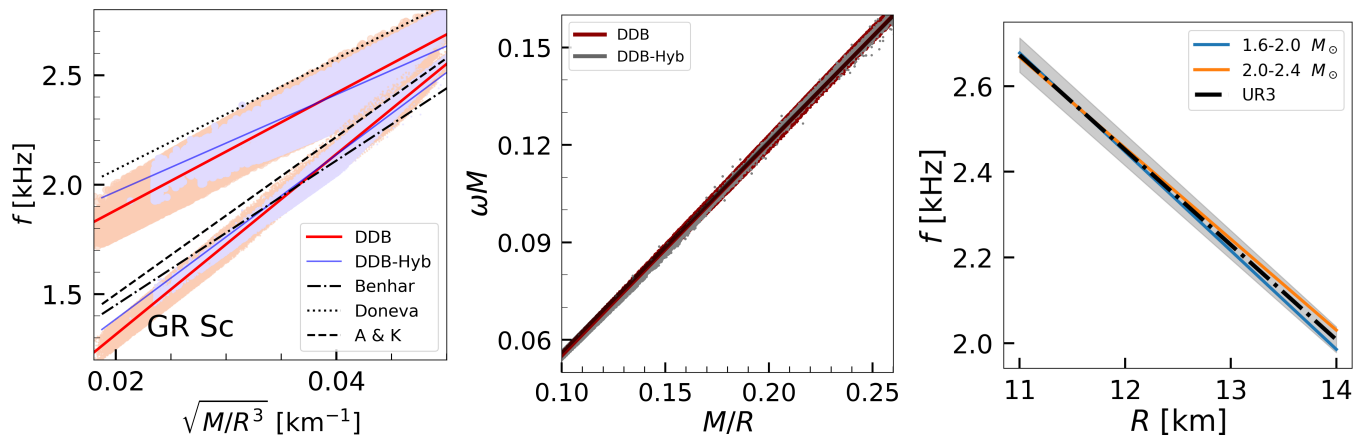


FIG. 3. URs obtained with our sets of EOSs, namely DDB-Hyb and DDB. UR1 (left): The frequency of the f mode is plotted as a function of the square root of the average density, and corresponding GR scaled data according to [51] (bottom band) as explained in the text. Also included are results from Doneva *et al.* [49] obtained in the Cowling approximation, Andersson & Kokkotas [19] and Benhar *et al.* [20] calculated with full GR; UR2a (center): The universality among ωM and M/R obtained with both datasets; and UR3 (right) the universal linear relations among f mode frequency and radii of NS with masses ranging from 1.6 to 2.4 M_{\odot} in a step of $0.2M_{\odot}$. The band corresponds to 90% CI

with a few nucleonic and hyperonic EOSs as $a = 0.65765$ and $b = 0.0127866$, respectively. We have also obtained a relation as UR2b for ωR as $\omega R = a \left(\frac{M}{R}\right)^2 + b \left(\frac{M}{R}\right) + c$. The coefficients are found to be $a = -3.0369 \pm 0.0013 (-3.1844 \pm 0.0020)$, $b = 1.5829 \pm 0.0005 (1.6288 \pm 0.0008)$ and $c = 0.4095 \pm 5 \times 10^{-5} (0.4087 \pm 7 \times 10^{-5})$ for DDB-Hyb (DDB) set, all the coefficients are dimensionless. In this case the maximum relative percentage error is 2.6% (1.6%) in the set DDB-Hyb (DDB). Compared with UR1, the relative maximum uncertainty is smaller for UR2a and UR2b for both DDB-Hyb and DDB sets. Using these relations we predict f mode frequencies for the PSR J0740+6620. For this pulsar, the mass and radius are determined as $2.08 \pm 0.7 M_{\odot}$ and 12.35 ± 0.75 km in [44] combining observational data from GW170817 and NICER as well as nuclear data. The corresponding mean values of f mode frequency is calculated as 2.35 kHz and 2.36 kHz for UR2a and UR2b, respectively, with a $\sim 1-4\%$ intrinsic error in the URs and additional $\sim 10-12\%$ error due to uncertainty present in mass and radius. A comment regarding the Cowling approximation may be in order.

We have identified a strong linear correlation between the f mode frequency and NS radius R and we are naming it as UR3. The values $r \in [0.98, 0.99]$ of the Pearson correlation coefficient were obtained between f and R for NS with a mass $M \in [1.6, 2.4]$ with our two sets of EOSs. These results can also be traced back from UR1 by keeping fixed NS mass while noting that the correlation is stronger only for the NS of large mass. In the right panel of Fig. 3, we plot the linear relations between f and R . The values of slope $m \in [-0.23, -0.21]$ and intercept are $c \in [5.21, 5.0]$ for NS mass $M \in [1.6 \text{ to } 2.0, 2.0 \text{ to } 2.4] M_{\odot}$. We also plot a marginalized UR3 obtained with NS masses in the range of 1.6 to 2.4 M_{\odot} with a slope, ($m = -0.22$) and an intercept, ($c = 5.1$). This gives $\approx 1.5\%$ relative residual within 90% CI.

We expect that the correlation is also present if the full GR solutions are considered. Taking this correction factor into account, the new relation (UR3) will be very useful for the upcoming future detection in order to constrain NS radius of massive NS precisely. For example, in order to measure a radius of a NS with ~ 0.2 km uncertainty, the f mode frequency needs to be measured within $\sim 2\%$ uncertainty.

Summary and conclusion - The QNMs are related with the viscous properties of matter. In the future, precise measurements of them can put constraints on the EOS of dense matter. We have studied the f mode frequency among the QNMs, which is in the sensitivity band of the future gravitational waves networks [17]. We have calculated the f mode frequency within the Cowling approximation with a nucleonic set of 14,000 EOSs (DDB set), obtained in Ref. [34] based on the relativistic mean field (RMF) theory, constrained by existing observational, theoretical and experimental data through Bayesian analysis. We have also generated an ensemble of EOSs using DDB below twice saturation density ($\rho \leq 2\rho_0$) and pQCD at high densities ($\rho \geq \rho_0$) as in Ref.[9]. Two piecewise polytropes have been used to interpolate the region from $2\rho_0$ to $40\rho_0$. Implementing the constraints of causality and maximum mass $M_{\max} \geq 2.0M_{\odot}$ a set of 55000 DDB-Hyb typed EOSs has obtained. The mass-radius cloud that we obtain from the ensembles of these EOSs is consistent with the GW170817 joint probability distribution as well as the recent NICER observations of mass and radius. We have analyzed the robustness of a few previously known universal relations, UR1 and UR2, and confirmed the robustness of UR2. UR1 shows a dispersion of 5% relative uncertainty at 90% CI, and a 15% smaller slope for the DDB-Hyb compared with the DDB set. We also found a novel strong correlation between the f mode frequency, f , and the radius, R , for a NS of mass in the range (1.6-2.4) M_{\odot} . These new direct relations between

f and R will allow an accurate determination of the radius of NS using future f mode detection.

We show that the quadrupolar f mode frequencies obtained in Cowling approximation of NS of masses $2.0M_{\odot}$ and above lie in the range (2.1-2.7) kHz and (2.3-2.65) kHz for DDB-Hyb and DDB sets, respectively. We use this URs to predict the f mode frequencies of the NICER observations and obtain ~ 2.35 (2.0) kHz in Cowling approximation (linearized GR) for the PSR J0740+6620 which interestingly lies within the sensitivity band of the future gravitational wave detector networks [17] for the detection of gravitational waves. It was shown that a two solar mass star with a low f mode frequency may indicate the existence of non-nucleonic degrees of freedom. In the future, a detailed investigation of how this frequency is correlated with the individual component of the EOS or different particle compositions in NS core will be carried out.

Acknowledgments- The authors acknowledge the Laboratory for Advanced Computing at the University of Coimbra for providing HPC resources for this research results reported within this paper, URL: <https://www.uc.pt/lca>. T.M and C.P would like to thank national funds from FCT (Fundação para a Ciência e a Tecnologia, I.P, Portugal) under Projects No. UID/FIS/04564/2019, No. UIDP/04564/2020, No. UIDB/04564/2020, and No. POCI-01-0145-FEDER-029912 with financial support from Science, Technology, and Innovation, in its FEDER component, and by the FCT/MCTES budget through national funds (OE).

* deepakk@prl.res.in

† tuhin.malik@uc.pt

‡ hiranmaya@niser.ac.in

- [1] N. K. Glendenning, *Compact Stars* (Springer New York, NY, 1996).
- [2] P. Haensel, A. Y. Potekhin, and D. G. Yakovlev, *Neutron Stars I : Equation of State and Structure*, Vol. 326 (Springer New York, NY, 2007).
- [3] L. Rezzolla, P. Pizzochero, D. I. Jones, N. Rea, and I. Vidaña, eds., *The Physics and Astrophysics of Neutron Stars*, Vol. 457 (Springer, 2018).
- [4] J. Schaffner-Bielich, *Compact Star Physics* (Cambridge University Press, 2020).
- [5] L. Lindblom and N. M. Indik, *Phys. Rev. D* **86**, 084003 (2012), [arXiv:1207.3744 \[astro-ph.HE\]](https://arxiv.org/abs/1207.3744).
- [6] A. Kurkela, E. S. Fraga, J. Schaffner-Bielich, and A. Vuorinen, *Astrophys. J.* **789**, 127 (2014), [arXiv:1402.6618 \[astro-ph.HE\]](https://arxiv.org/abs/1402.6618).
- [7] E. R. Most, L. R. Weih, L. Rezzolla, and J. Schaffner-Bielich, *Phys. Rev. Lett.* **120**, 261103 (2018), [arXiv:1803.00549 \[gr-qc\]](https://arxiv.org/abs/1803.00549).
- [8] E. Lope Oter, A. Windisch, F. J. Llanes-Estrada, and M. Alford, *J. Phys. G* **46**, 084001 (2019), [arXiv:1901.05271 \[gr-qc\]](https://arxiv.org/abs/1901.05271).
- [9] E. Annala, T. Gorda, A. Kurkela, J. Nättilä, and A. Vuorinen, *Nature Phys.* **16**, 907 (2020), [arXiv:1903.09121 \[astro-ph.HE\]](https://arxiv.org/abs/1903.09121).
- [10] E. Annala, T. Gorda, E. Katerini, A. Kurkela, J. Nättilä, V. Paschalidis, and A. Vuorinen, *Phys. Rev. X* **12**, 011058 (2022), [arXiv:2105.05132 \[astro-ph.HE\]](https://arxiv.org/abs/2105.05132).
- [11] S. Altıparmak, C. Ecker, and L. Rezzolla, *Astrophys. J. Lett.* **939**, L34 (2022), [arXiv:2203.14974 \[astro-ph.HE\]](https://arxiv.org/abs/2203.14974).
- [12] P. B. de Tovar, M. Ferreira, and C. Providência, *Phys. Rev. D* **104**, 123036 (2021), [arXiv:2112.05551 \[nucl-th\]](https://arxiv.org/abs/2112.05551).
- [13] S. M. A. Imam, N. K. Patra, C. Mondal, T. Malik, and B. K. Agrawal, *Phys. Rev. C* **105**, 015806 (2022), [arXiv:2110.15776 \[nucl-th\]](https://arxiv.org/abs/2110.15776).
- [14] C. Mondal and F. Gulminelli, *Phys. Rev. D* **105**, 083016 (2022), [arXiv:2111.04520 \[nucl-th\]](https://arxiv.org/abs/2111.04520).
- [15] R. Essick, I. Tews, P. Landry, and A. Schwenk, *Phys. Rev. Lett.* **127**, 192701 (2021).
- [16] C. Chirenti, P. R. Silveira, and O. D. Aguiar, *Int. J. Mod. Phys. Conf. Ser.* **18**, 48 (2012), [arXiv:1205.2001 \[gr-qc\]](https://arxiv.org/abs/1205.2001).
- [17] G. Pratten, P. Schmidt, and T. Hinderer, *Nature Commun.* **11**, 2553 (2020), [arXiv:1905.00817 \[gr-qc\]](https://arxiv.org/abs/1905.00817).
- [18] N. Andersson and K. D. Kokkotas, *Phys. Rev. Lett.* **77**, 4134 (1996), [arXiv:gr-qc/9610035](https://arxiv.org/abs/gr-qc/9610035).
- [19] N. Andersson and K. D. Kokkotas, *Mon. Not. Roy. Astron. Soc.* **299**, 1059 (1998), [arXiv:gr-qc/9711088](https://arxiv.org/abs/gr-qc/9711088).
- [20] O. Benhar, E. Berti, and V. Ferrari, *Mon. Not. Roy. Astron. Soc.* **310**, 797 (1999), [arXiv:gr-qc/9901037](https://arxiv.org/abs/gr-qc/9901037).
- [21] O. Benhar, V. Ferrari, and L. Gualtieri, *Phys. Rev. D* **70**, 124015 (2004), [arXiv:astro-ph/0407529](https://arxiv.org/abs/astro-ph/0407529).
- [22] L. K. Tsui and P. T. Leung, *Mon. Not. Roy. Astron. Soc.* **357**, 1029 (2005), [arXiv:gr-qc/0410204](https://arxiv.org/abs/gr-qc/0410204).
- [23] T. K. Chan, Y. H. Sham, P. T. Leung, and L. M. Lin, *Phys. Rev. D* **90**, 124023 (2014), [arXiv:1408.3789 \[gr-qc\]](https://arxiv.org/abs/1408.3789).
- [24] H. Sotani, *Phys. Rev. D* **103**, 123015 (2021), [arXiv:2105.13212 \[astro-ph.HE\]](https://arxiv.org/abs/2105.13212).
- [25] H. Sotani and B. Kumar, *Phys. Rev. D* **104**, 123002 (2021), [arXiv:2109.08145 \[gr-qc\]](https://arxiv.org/abs/2109.08145).
- [26] P. N. McDermott, H. M. van Horn, and J. F. Scholl, *Astrophys. J.* **268**, 837 (1983).
- [27] S. Yoshida and U. Lee, *Astron. Astrophys.* **395**, 201 (2002), [arXiv:astro-ph/0210591](https://arxiv.org/abs/astro-ph/0210591).
- [28] S. Y. Lau, P. T. Leung, and L. M. Lin, *Phys. Rev. D* **99**, 023018 (2019), [arXiv:1808.08107 \[astro-ph.HE\]](https://arxiv.org/abs/1808.08107).
- [29] D. Bandyopadhyay, S. A. Bhat, P. Char, and D. Chatterjee, *Eur. Phys. J. A* **54**, 26 (2018), [arXiv:1712.01715 \[astro-ph.HE\]](https://arxiv.org/abs/1712.01715).
- [30] S. Han and A. W. Steiner, *Phys. Rev. D* **99**, 083014 (2019), [arXiv:1810.10967 \[nucl-th\]](https://arxiv.org/abs/1810.10967).
- [31] P. von Doetinchem *et al.*, *JCAP* **08**, 035 (2020), [arXiv:2002.04163 \[astro-ph.HE\]](https://arxiv.org/abs/2002.04163).
- [32] G. Baym, C. Pethick, and P. Sutherland, *Astrophys. J.* **170**, 299 (1971).
- [33] J. Carriere, C. J. Horowitz, and J. Piekarewicz, *Astrophys. J.* **593**, 463 (2003), [arXiv:nucl-th/0211015](https://arxiv.org/abs/nucl-th/0211015).
- [34] T. Malik, M. Ferreira, B. K. Agrawal, and C. Providência, *Astrophys. J.* **930**, 17 (2022), [arXiv:2201.12552 \[nucl-th\]](https://arxiv.org/abs/2201.12552).
- [35] I. Tews, T. Krüger, K. Hebeler, and A. Schwenk, *Phys. Rev. Lett.* **110**, 032504 (2013), [arXiv:1206.0025 \[nucl-th\]](https://arxiv.org/abs/1206.0025).
- [36] K. Hebeler, J. M. Lattimer, C. J. Pethick, and A. Schwenk, *Astrophys. J.* **773**, 11 (2013), [arXiv:1303.4662 \[astro-ph.SR\]](https://arxiv.org/abs/1303.4662).
- [37] A. Kurkela, P. Romatschke, and A. Vuorinen, *Phys. Rev. D* **81**, 105021 (2010), [arXiv:0912.1856 \[hep-ph\]](https://arxiv.org/abs/0912.1856).
- [38] E. S. Fraga, A. Kurkela, and A. Vuorinen, *Astrophys. J. Lett.* **781**, L25 (2014), [arXiv:1311.5154 \[nucl-th\]](https://arxiv.org/abs/1311.5154).
- [39] A. Florian, *Probabilistic Engineering Mechanics* **7**, 123 (1992).
- [40] L. Lindblom, *Phys. Rev. D* **82**, 103011 (2010), [arXiv:1009.0738 \[astro-ph.HE\]](https://arxiv.org/abs/1009.0738).
- [41] L. Lindblom, *Phys. Rev. D* **97**, 123019 (2018), [arXiv:1804.04072 \[astro-ph.HE\]](https://arxiv.org/abs/1804.04072).
- [42] E. Annala, T. Gorda, A. Kurkela, J. Nättilä, and A. Vuorinen, *Nature Phys.* **16**, 907 (2020), [arXiv:1903.09121 \[astro-ph.HE\]](https://arxiv.org/abs/1903.09121).
- [43] D. Kumar, H. Mishra, and T. Malik, *JCAP* **02**, 015 (2023),

- arXiv:2110.00324 [hep-ph].
- [44] M. C. Miller *et al.*, *Astrophys. J. Lett.* **918**, L28 (2021), arXiv:2105.06979 [astro-ph.HE].
- [45] B. P. Abbott *et al.* (LIGO Scientific, Virgo), *Phys. Rev. X* **9**, 011001 (2019), arXiv:1805.11579 [gr-qc].
- [46] T. E. Riley *et al.*, *Astrophys. J. Lett.* **887**, L21 (2019), arXiv:1912.05702 [astro-ph.HE].
- [47] M. C. Miller *et al.*, *Astrophys. J. Lett.* **887**, L24 (2019), arXiv:1912.05705 [astro-ph.HE].
- [48] T. E. Riley *et al.*, *Astrophys. J. Lett.* **918**, L27 (2021), arXiv:2105.06980 [astro-ph.HE].
- [49] D. D. Doneva, E. Gaertig, K. D. Kokkotas, and C. Krüger, *Phys. Rev. D* **88**, 044052 (2013), arXiv:1305.7197 [astro-ph.SR].
- [50] B. K. Pradhan, D. Chatterjee, M. Lanoye, and P. Jaikumar, *Phys. Rev. C* **106**, 015805 (2022), arXiv:2203.03141 [astro-ph.HE].
- [51] S. Yoshida and Y. Kojima, *Mon. Not. Roy. Astron. Soc.* **289**, 117 (1997), arXiv:gr-qc/9705081.
- [52] K. D. Kokkotas, T. A. Apostolatos, and N. Andersson, *Mon. Not. Roy. Astron. Soc.* **320**, 307 (2001), arXiv:gr-qc/9901072.
- [53] B. K. Pradhan and D. Chatterjee, *Phys. Rev. C* **103**, 035810 (2021), arXiv:2011.02204 [astro-ph.HE].